The Planetary Science Journal, 6:287 (10pp), 2025 December https://doi.org/10.3847/PSJ/ae2022

Using SOFIA's EXES to Search for C_6H_2 and C_4N_2 in Titan's Atmosphere

Zachary C. McQueen[1,2], Conor A. Nixon[1], Curtis de Witt[3], Véronique Vuitton[4], Panayotis Lavvas[5], Juan Alday[6], Nicholas A. Teanby[7], Joseph Penn[8], Antoine Jolly[9], and Patrick G. J. Irwin[8]
[1] NASA Goddard Space Flight Center, 8800 Greenbelt Rd., Greenbelt, MD 20771, USA
[2] Southeast Universities Research Association, 1201 New York Ave., Suite 430, Washington, DC 20005, USA
[3] Space Science Institute, 4765 Walnut St. STE B, Boulder, CO 80301, USA
[4] Univ. Grenoble Alpes, CNRS, IPAG, 38000 Grenoble, France
[5] GSMA UMR 7331, University Reims Champagne Ardenne, Reims, France
[6] Instituto de Astrofísica de Andalucía, CSIC, Granada, Spain
[7] University of Bristol, Queens Rd., Clifton, Bristol BS8 1RJ, UK
[8] Oxford University, Clarendon Laboratory, Parks Rd., Oxford OX1 3PU, UK
[9] Université Paris Est Créteil and Université Paris Cité, Créteil, France
Received 2025 September 22; revised 2025 November 12; accepted 2025 November 13; published 2025 December 11

Abstract

In Titan's atmosphere, the chemistry of simple hydrocarbons (e.g., CH_4 and C_2H_2) and nitrogen bearing species (e.g., N_2 and CN) represents an important link between molecular species and the ubiquitous organic haze that gives Titan its characteristic orange hue. Here we present a new search for two previously undetected molecules, triacetylene (C_6H_2) and the gas phase dicyanoacetylene (C_4N_2), using the Echelon-Cross-Echelle Spectrograph instrument on board the Stratospheric Observatory for Infrared Astronomy aircraft. We do not detect these two molecules but determine upper limits for their mixing ratios and column abundances. We find the 3σ upper limits on the uniform volume mixing ratio (VMR) above 100 km for C_6H_2 to be 4.3×10^{-11}, which is lower than the photochemical model predictions. This new upper limit suggests that the growth of linear molecules is inhibited. We also put a strict upper limit on the uniform VMR for gas phase C_4N_2 above 125 km to be 1.0×10^{-10}. This upper limit is well below the saturation mixing ratio at this altitude for C_4N_2 and greatly limits the feasibility of C_4N_2 forming ice from condensation.

Unified Astronomy Thesaurus concepts: Titan (2186); Natural satellite atmospheres (2214); Infrared spectroscopy (2285); Infrared astronomy (786); Atmospheric composition (2120)

1. Introduction

Titan's major atmospheric components, N_2 (nitrogen) and CH_4 (methane), photodissociate and ionize in Titan's ionosphere, consequentially leading to the formation of other hydrocarbon and nitrile species (S. M. Hörst 2017; C. A. Nixon 2024). These minor components continue this photochemical process, leading to larger and more complex organic species and ultimately the formation of Titan's characteristic haze (M. G. Trainer et al. 2006; J. H. Waite et al. 2007). Discovery of Titan's gaseous atmosphere came from early observations of Titan using Earth-based astronomy, where G. P. Kuiper (1944) discovered the presence of CH_4. The Voyager 1 flyby then confirmed the bulk of Titan's atmosphere was composed of N_2, and infrared observations of Titan's atmosphere from both Voyager 1 and Voyager 2 flybys allowed for the discovery of a wealth of new trace species (A. L. Broadfoot et al. 1981; R. Hanel et al. 1981; W. C. Maguire et al. 1981; R. E. Samuelson et al. 1983; B. Letourneur & A. Coustenis 1993). Space based observatories, like the Infrared Space Observatory, also contributed greatly to discovering new trace gases in Titan's atmosphere, including water and benzene (A. Coustenis et al. 1998, 2003; T. Encrenaz 2003). The return to Titan with the Cassini–Huygens mission provided excellent spatial, temporal, and vertical coverage of Titan's atmosphere (A. Coustenis et al. 2010; C. A. Nixon et al. 2019), allowing for several detailed IR studies of Titan over several seasons (e.g., N. Teanby et al. 2008; S. Vinatier et al. 2015; N. A. Lombardo et al. 2019a; N. A. Teanby et al. 2019; S. Vinatier et al. 2020; L. Wright et al. 2025). Following the conclusion of the Cassini–Huygens mission, Earth-based observations at infrared and submillimeter wavelengths have been a major contributor to searching for and detecting trace gases that are predicted to be present in Titan's atmosphere at low abundances (M. Y. Palmer et al. 2017; M. A. Cordiner et al. 2019; N. A. Lombardo et al. 2019b; A. E. Thelen et al. 2019; M. A. Cordiner et al. 2020; C. A. Nixon et al. 2020). Most recently, observations using the James Webb Space Telescope have allowed for the recent discovery of the CH_3 radical in Titan's atmosphere (C. A. Nixon et al. 2025), showing the importance of continued searches for trace gases that connect the many chemical mechanisms in Titan's atmosphere.

Polyynes or polyacetylenes are linear chains of acetylene groups and bear the molecular formula $C_{2n}H_2$ where $n \geqslant 2$. Polyynes represent one potential pathway to form macromolecules in Titan's atmosphere that bridge the gap between simple molecules and Titan's aerosols (E. Chassefière & M. Cabane 1995; S. Lebonnois et al. 2002). Polyynes form readily through the addition of the ethynyl radical (C_2H) to the precursor acetylene (C_2H_2) or polyacetylene molecule, i.e., diacetylene C_4H_2 (X. Gu et al. 2009). Although polyynes have been observed in the interstellar medium (J. Cernicharo et al. 2001a, 2001b), and are predicted to form in Titan's atmosphere at observable abundances (X. Gu et al. 2009; V. Vuitton et al. 2019), C_4H_2 is the highest-order polyyne that has been detected in Titan's atmosphere (V. G. Kunde et al. 1981; N. Teanby et al. 2009). Triacetylene (C_6H_2), which

Table 1
Description of EXES Observations of Titan's Atmosphere

Target, Setting (cm^{-1})	Date (yyyy-mm-dd)	Altitude (feet)	Air Mass	Distance (au)	D_v ($km\ s^{-1}$)	Integration Time (s)
Callisto, 621	2021-06-09	43,000	1.84	⋯	⋯	1408
Titan, 621	2021-06-09	43,000	1.68	9.321	−20.994	1504
Vesta, 472	2021-06-11	39,000	1.68	⋯	⋯	1504
Titan, 472	2021-06-15	43,000	1.84	9.264	−18.930	1600
Titan, 472	2021-06-17	43,000	1.67	9.240	−22.499	2560
Titan, 472	2021-12-04	36,000	2.00	10.424	+28.940	3392

forms from C_4H_2, is predicted in photochemical models to have a stratospheric abundance of 0.6 ppb (V. Vuitton et al. 2019), yet to this date the spectroscopic detection of C_6H_2 has eluded the community.

There have been two previous studies of Titan's C_6H_2 upper limits. The first upper limit of C_6H_2, reported by C. Delpech et al. (1994), was determined by comparing the expected signal intensity from the strongest vibrational mode of C_6H_2 to the observed emission features of a reference compound and was found to be 0.6 ppb above 100 km. This study was in agreement with the photochemical model predictions at the time, but was limited by the low spectral resolution of Voyager's Infrared Interferometer Spectrometer and Radiometer (IRIS), and the authors note that a higher-resolution spectrometer may allow C_6H_2 to be detected. F. Shindo et al. (2003) updated measurements of the C_6H_2 IR spectrum and recalculated the upper limits and lowered them to 0.44 ppb above 150 km using a similar method. Still, at these upper limits, C_6H_2 and higher-order polyynes represent a potential pathway to the formation of large hydrocarbons in Titan's atmosphere. Therefore, an updated analysis of the upper limits for C_6H_2 at high spectral resolution will provide useful estimations of the potential for higher-order polyyne formation in Titan's atmosphere.

Dicyanoacetylene (C_4N_2) in the gas phase is predicted to form in Titan's atmosphere through the reaction of HC_3N with CN (V. Vuitton et al. 2019). This was recently shown to occur in crossed molecular beam experiments by E. V. F. de Aragão (2025). Additionally, C_4N_2 can form through HCN reaction with C_3N and through hydrogen elimination of HC_4N_2, though HC_4N_2 is formed following C_4N_2 formation (J. Loison et al. 2015). C_4N_2 is unique in Titan's atmosphere because, although the gas phase species has not been detected, C_4N_2 ice has been reported in both Voyager's IRIS spectra and Cassini's Composite Infrared Spectrometer (CIRS) spectra (R. Samuelson et al. 1997; C. M. Anderson et al. 2016). Following the Voyager flyby, an emission feature at 478 cm^{-1} was assigned to the ice-phase ν_8 vibrational mode of C_4N_2; however, the gas phase emission at 471 cm^{-1} was not present. Some years later, the same anomalous feature at 478 cm^{-1} arose in CIRS observations of Titan's atmosphere and was also assigned to C_4N_2 ice. Since then, there have been several studies attempting to understand why this ice feature is so strong but the gas is not present in detectable amounts. R. Samuelson et al. (1997) suggested that the gas phase C_4N_2 is enriched during the winter, leading to condensation, and then photochemically consumed rapidly at the spring equinox while the condensate progressively builds up in the lower stratosphere. This, however, was suggested not to be feasible by R. de Kok et al. (2008), as their upper limit of 1×10^8, before equinox, was too small to allow for ice formation even under the rapid depletion scenario.

The most recent hypothesis for C_4N_2 ice formation in Titan's atmosphere was presented in C. M. Anderson et al. (2016) where, rather than C_4N_2 ice forming directly from condensation, it is formed completely via solid-state photochemistry within HCN-HC_3N ice mixtures. This proposed mechanism, however, requires a column abundance of 10^{17} molecules cm^{-2} to obtain a good spectral fit to the 478 cm^{-1} emission feature. Such a high column abundance is larger than the simpler, but related, molecule, cyanogen (C_2N_2), which has been detected in Titan's atmosphere (V. G. Kunde et al. 1981; J. Loison et al. 2015). Updated estimations of the upper limits on the gas phase abundance of C_4N_2 will help constrain the feasibility of C_4N_2 ice formation in Titan's atmosphere.

In the present study, we use high-resolution ($R \sim 90{,}000$) mid-IR spectroscopy with observations made by the Echelon-Cross-Echelle Spectrograph (EXES) on board the Stratospheric Observatory for Infrared Astronomy (SOFIA) aircraft at two spectral settings, 621 and 472 cm^{-1}, to search for C_6H_2 and C_4N_2, respectively. We apply radiative transfer models to fit the measured spectra and retrieve the atmospheric abundances of C_4H_2 and C_3H_4 in order to derive upper limits for the undetected species, C_6H_2 and C_4N_2. We then compare these upper limits to photochemical model predictions of the target species and discuss the implications these upper limits have on our understanding of Titan's atmospheric chemistry.

2. EXES Observations

Observations of Titan's atmospheric spectra were made using EXES on board NASA's SOFIA aircraft (M. J. Richter et al. 2018). Details of the observations are listed in Table 1. Spectra were collected during flights 744 and 746 in 2021 June. EXES was operated in a high-medium configuration to obtain high-resolution ($R \sim$ 75,000–90,000) spectra centered at 472 and 621 cm^{-1} to observe the emission features of C_4N_2 for the former and C_4H_2, C_6H_2, and C_3H_4 for the latter region. Targets were nodded along the slit in an ABAB pattern by 7″–8″ at intervals of 4 minutes to facilitate sky background subtraction.

The 2.″65 slit width was used for the 621 cm^{-1} setting. Even at SOFIA's altitude, the telluric spectrum at 621 cm^{-1} has interference from densely spaced atmospheric lines of CO_2, O_3, and N_2O. To enable removal of these features, Callisto (the telluric calibrator) and Titan were observed on adjacent flight legs, at the same altitude and with an air-mass difference of 0.16, ensuring the best possible match in telluric transmission. To accurately model the instrument line shape, we derived the resolving power of the measurement by fitting synthetic transmission models to the Callisto spectrum, which were generated by Planetary Spectrum Generator (PSG;

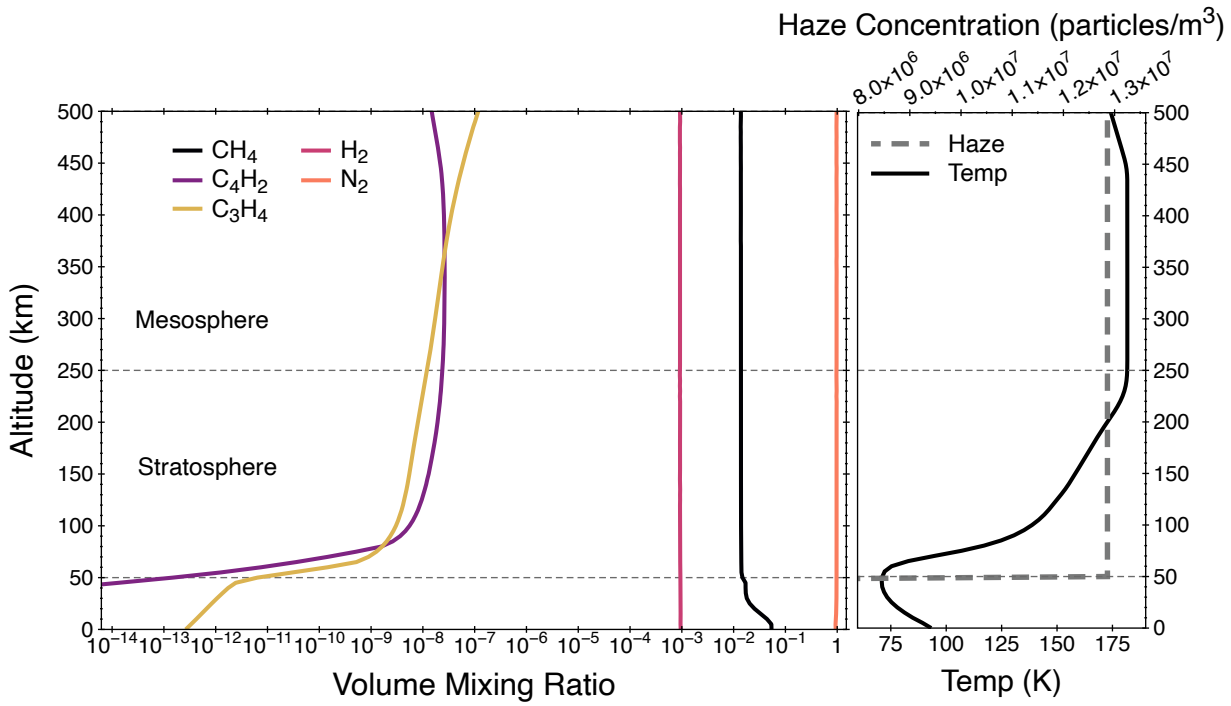

Figure 1. Reference profiles of the atmospheric gas composition (left panel), vertical temperature profile (right panel, solid black trace), and haze profiles (gray dashed trace). Temperature and gas profiles are from the photochemical model detailed in V. Vuitton et al. (2019).

G. L. Villanueva et al. 2018). We found the resolving power at the 621 cm^{-1} spectral setting to be $R = 90000 \pm 2500$.

The 472 cm^{-1} observations were taken on three flights with a slit width of 3.″2. Due to the low density of telluric atmosphere features near 472 cm^{-1}, telluric interference was a minor issue that could be addressed by synthetic PSG atmosphere models and masking the regions containing features due to water. The telluric calibrator, Vesta, was observed for this setting to mitigate risk, but it was only used to derive a resolving power for the 472 cm^{-1} setting, $R = 75{,}000 \pm 2500$.

All data were reduced with the EXES Redux pipeline (M. Clarke et al. 2015) version 3.0.1.dev.7 with the customary steps including spike removal, flat-fielding, rectification of the cross-dispersed orders, coadding of nod pairs, and extraction to the 1D using optimal point-spread function weighting. Following data reduction using the Redux pipeline, spectral data points were binned using Nyquist sampling to a $\Delta\bar{\nu} = 0.003$ in order to reduce the noise in the spectrum.

3. Radiative Transfer Modeling

Spectra were modeled using the archNEMESIS (J. Alday et al. 2025) radiative transfer model, which is a Python implementation of the Nonlinear Optimal Estimator for Multivariate Spectral Analysis (NEMESIS; P. Irwin et al. 2008). NEMESIS has been used extensively to model Titan atmospheric spectra (C. A. Nixon et al. 2013; N. A. Lombardo et al. 2019b; N. A. Teanby et al. 2019; A. E. Thelen et al. 2019; L. Wright et al. 2024) and has been used for modeling observations of Titan made with the Texas Echelon-Cross-Echelle Spectrometer (TEXES), the sister instrument to EXES (N. A. Lombardo et al. 2019b). archNEMESIS allows for both multicore processing and larger spectral datasets due to improved memory efficiency in Python.

For this study, archNEMESIS is employed in two different ways to model the target species. First, the spectra are inverted using the optimal estimation method to retrieve the continuous atmospheric profiles of C_4H_2 and C_3H_4 (for the 621 cm^{-1} spectral setting) as well as the scaling factor for Titan's haze profile (both spectral settings). We retrieved continuous profiles for the known gases (C_4H_2 and C_3H_4) and a scaling factor for the haze profile. We used an atmospheric model with 100 homogeneous layers equally spaced in log pressure to sufficiently sample the vertical profile of Titan's atmosphere. The a priori reference atmosphere used, shown in Figure 1, uses gas and temperature profiles described in the V. Vuitton et al. (2019) photochemical model. The photochemical model profiles for C_4H_2 and C_3H_4 were each scaled by 0.2 and 0.5, respectively, prior to retrieving the continuous profiles to ensure a good fit to the spectrum was achieved. To fit the continuum level, we retrieved a scaling factor for a uniform haze profile with an a priori concentration of 1.29×10^7 particles m^{-3} above 50 km (Figure 1), using a uniform cross section across the wavelength range for both spectra.

Since the EXES observations are of Titan's disk, we modeled these observations using a weighted average of emission rays from different emission angles of the solid body and emission rays from the limb. We followed a similar approach to N. Teanby et al. (2013) to both sufficiently sample Titan's radiance and calculate weights for each emission ray. In total, we used 55 emission rays from the disk center out to a limb height of 975 km.

3.1. Spectroscopic Data

Spectra were calculated in line-by-line mode using pre-tabulated line-by-line lookup tables calculated at 30 pressure and temperature levels between 5.6×10^{-9}–2.5 bar and 70–250 K. Line data were then interpolated to the pressures and temperatures at each atmospheric layer in the atmospheric

Table 2
Literature Values for the Infrared Band Intensities of the Molecules Investigated

Molecule	Band	Position (cm^{-1})	Absolute Intensity (atm^{-1} cm^{-2})	References
C_6H_2	ν_{11}	622	428 ± 25	F. Shindo et al. (2003)
C_4H_2	ν_8	628	563 ± 23	A. Jolly et al. (2014)
C_3H_4	ν_9	638	⋯	K. Pekkala (1990)
C_4N_2	ν_8	471.6	52 ± 1.5	A. Jolly et al. (2015)

model. Spectra were also calculated using a Gaussian line shape at the resolving power of each spectral setting. The spectroscopic line lists for the known gas emission features at the 621 cm^{-1} spectral setting, namely the ν_8 band of C_4H_2 and the ν_9 band of C_3H_4, were obtained from the HITRAN (I. Gordon et al. 2022) and GEISA (T. Delahaye et al. 2021) spectroscopic databases, respectively. All band intensities for the observed and targeted emission features are listed in Table 2, with the exception of the band intensity of the ν_9 band of C_3H_4, not reported in K. Pekkala (1990). Both target species for this study, C_6H_2 and C_4N_2, are less commonly measured in atmospheric spectra and are not available in the standard databases; however, their infrared spectra have been well characterized in laboratory settings. F. Shindo et al. (2003) measured the mid-infrared spectrum of C_6H_2 and is the most up-to-date line list for the ν_{11} band at ~622 cm^{-1}. This band is an intense, out-of-plane bending mode that is centered in a window ideal for being targeted by EXES. The ν_5 band is more intense, but the Q-branch is centered at 3322 cm^{-1} where the Titan spectra are opaque due to strong absorption from CH_4. Similarly, A. Jolly et al. (2015) obtained the line list for the ν_8 bending mode of C_4N_2 in a previous investigation of the upper limits of the gas phase species in Titan's atmosphere. This ν_8 is covered by the EXES spectral bandwidth, but is less intense than the ν_9 vibrational mode, centered at 107 cm^{-1} (A. Jolly et al. 2015), which is outside of the EXES spectral window. Additionally, the emission features for both target species were targeted during the SOFIA mission specifically because the 621 and 472 cm^{-1} spectral windows are blocked from the surface due to CO_2 and H_2O absorption in the Earth's atmosphere. Data for collision-induced absorption were obtained from the 2025 HITRAN database update (J. Terragni et al. 2025).

3.2. Determining Upper Limits

Following the spectral fit, we determine the upper limits to the C_6H_2 and C_4N_2 abundance. We determine the goodness of fit for the modeled spectrum by summing the ratio of the square residual of the fit to the squared uncertainty of the measurement, described in Equation (1),

$$\chi^2 = \frac{\Delta\bar{\nu}_{\rm obs}}{\Delta\bar{\nu}_{\rm res}} \sum_{i=1}^{M} \frac{(I_m(\bar{\nu_i}) - I_r(\bar{\nu_i}))^2}{\sigma_i^2}, \quad (1)$$

where I_m and I_r are the spectral radiance for the measurement and retrieved spectrum, respectively, at wavenumber $\bar{\nu}_i$, and σ_i is the wavenumber-dependent uncertainty. Once the emission features of the spectral region are well fit, the remaining residual will be due to instrument noise and any unfit gas emission features that were not included in the retrieval. The vertical profile of the target species is then set to be a uniform volume mixing ratio (VMR) above a condensation altitude, and we iterate over a range of VMR values, calculating a forward model of the spectrum at each abundance, and determine the change in the χ^2, $\Delta\chi^2$, with increased abundance of the target species. If the gas is present in detectable amounts, $\Delta\chi^2$ will decrease significantly, indicating the spectral fit is improved with the inclusion of the target species. Alternatively, when $\Delta\chi^2$ increases, the upper limits can be determined at $\Delta\chi^2 = +1$, $+4$, and $+9$ for 1σ, 2σ, and 3σ upper limits, respectively. This method has been used in several previous studies of Titan's atmospheric trace constituents for detections and upper limits (N. Teanby et al. 2009; C. A. Nixon et al. 2010; A. Jolly et al. 2015).

4. Results

4.1. Abundance Retrievals for C_4H_2 and C_3H_4

To fit the measured spectra, we used the optimal estimation method for retrieving the vertical profiles of the gases, C_4H_2 and C_3H_4, known to have emission features in the 621 cm^{-1} spectral setting and a scaling factor for a uniform haze vertical profile at both spectral settings. The model fits to both spectra are shown in Figure 2. We obtained a good fit ($\chi^2/N = 0.999$) to the measured 621 cm^{-1} spectrum by fitting to the gas emission features of C_4H_2 and C_3H_4. The residual of the fit to the measurement is shown in the lower panel and is within the 1σ estimation of the instrument noise. At lower wavenumbers, some of the emission features are slightly overfit, and at longer wavenumbers the radiance of the stronger emission features is not fully captured; however, the overall fit is good. C_4H_2 exhibits the strongest peaks, indicated by the blue vertical lines, with emission features originating from the P-branch of the ν_8 vibrational mode. The emission features of C_3H_4, originating from the ν_9 vibrational mode, are less intense, but tightly bunched and often near emission features from C_4H_2. Previously, these individual emission lines would not have been resolved with lower-resolution spectrometers. At the 472 cm^{-1} spectral setting, we only modeled the continuum level of the spectrum as no clear emission features were present. Without fitting any gas emission features, the model produced a $\chi^2/N = 1.01$, indicating the spectrum does not contain any significant features that are not being fit by the model.

Figure 3 shows the retrieved continuous profiles of each fit species in the altitude region where the Jacobian is peaked. For each species, the model was most sensitive in the stratosphere and lower mesosphere between 80 and 275 km, where the majority of the gas abundance is found, peaking at ~130 km (~5×10^{-3} bar) for each species. Overall, the shape of the vertical profiles was retained in the retrieval; however, the retrieved profile for C_4H_2 is significantly lower than the V. Vuitton et al. (2019) photochemical model. This lower abundance is in better agreement with the J. Loison et al. (2019) predicted profile; however, the J. Loison et al. (2019) model underpredicts the abundance below 150 km in the stratosphere. Also shown in Figure 3 is the retrieved vertical profile from S. Vinatier et al. (2007), who retrieved the vertical profiles of several trace species from infrared spectra of Titan's limb collected by CIRS. The retrieval from the present work agrees well with S. Vinatier et al. (2007) at the probed altitudes. The retrieved profile for C_3H_4 was in better agreement with the V. Vuitton et al. (2019) prediction than that of C_4H_2. The retrieval was slightly lower than the prediction in the upper stratosphere (near 250 km), but a slight enhancement in the profile at the lower stratosphere brought

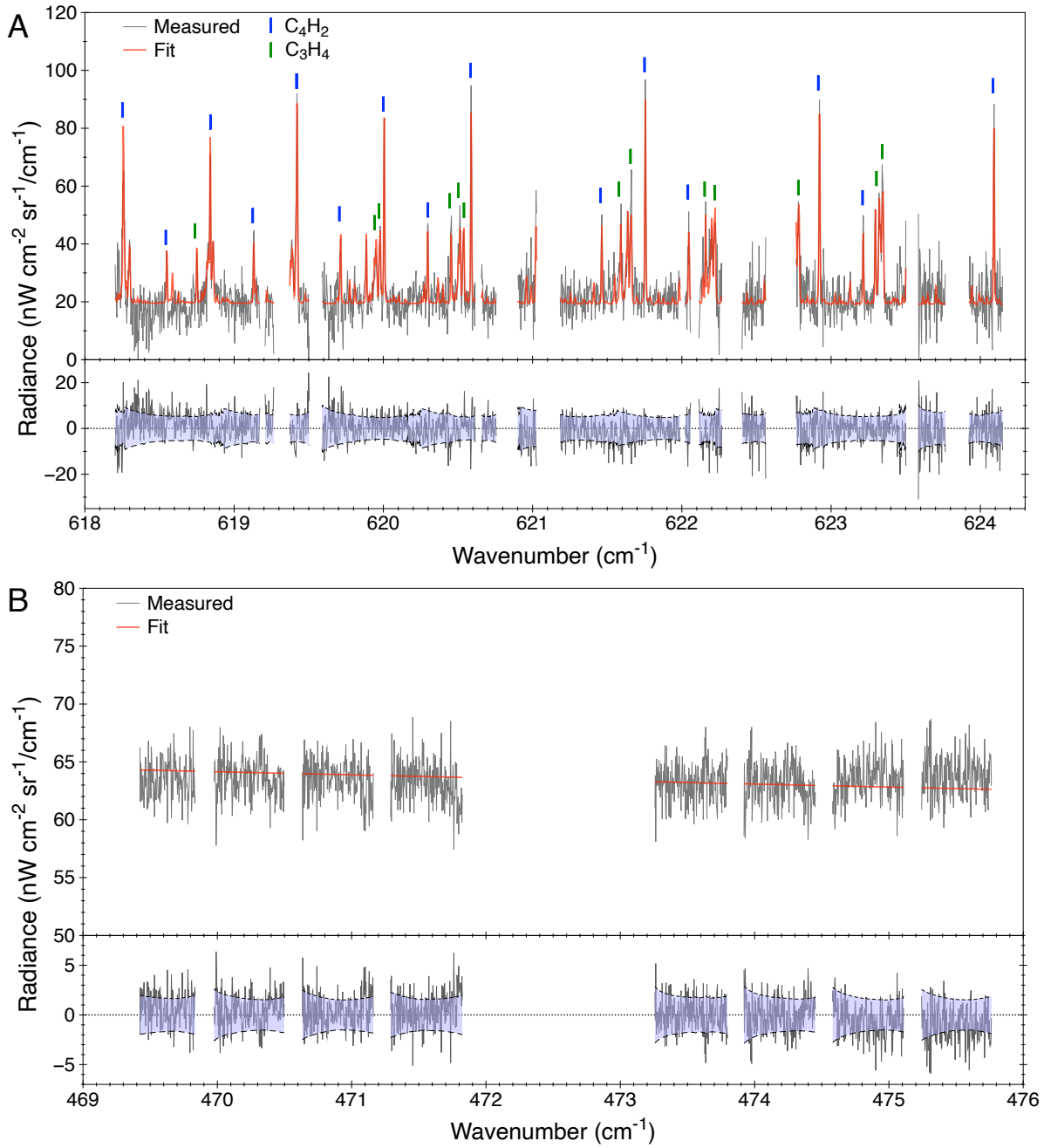

Figure 2. Model fit (red trace) to the measured spectrum (gray trace) for the 621 cm^{-1} (A) and 472 cm^{-1} (B) spectral settings. Bottom panels show the residual of the model fit to the measured spectra and a 1σ estimation of the instrument uncertainty in the blue shaded regions. Emission features from C_4H_2 and C_3H_4 are indicated by the respective markers in panel (A). There are no known emission features in the 472 cm^{-1} spectral setting, and only the haze and CIA continuum levels were fit in the retrieval.

the retrieval closer to the photochemical model prediction. This retrieved profile was also in good agreement with that of S. Vinatier et al. (2007), though the S. Vinatier et al. (2007) profile shows the consistent VMR of $\sim 5 \times 10^{-9}$ goes deeper in the atmosphere. The J. Loison et al. (2019) prediction agrees within the error estimation near 200 km, but underpredicts the C_3H_4 abundance below ~150 km.

4.2. Upper Limits for C_6H_2 and C_4N_2

Following the retrievals, we determine the upper limits of C_6H_2 and C_4N_2 by simulating multiple spectra with increasing abundance of the target species while keeping the retrieved profiles of the known gases and haze fixed. The difference between the χ^2 of the updated spectrum and the retrieved spectrum ($\Delta\chi^2$) is calculated at each abundance or scale factor. If the target species is present, the $\Delta\chi^2$ value will decrease significantly, indicating the spectrum is better fit. A rejection of the detection occurs when the $\Delta\chi^2$ increases sharply with increased abundance. Figure 4 shows the $\Delta\chi^2$ with increased VMR for C_6H_2 (A) and C_4N_2 (C). The cutoff altitude for C_6H_2 was set to 100 km, based on the condensation altitude reported in F. Shindo et al. (2003), who also performed an upper limits study of C_6H_2 using a similar profile. The $\Delta\chi^2$ dips slightly below zero with increased abundance of C_6H_2, but is nowhere near a significance level to indicate detection,

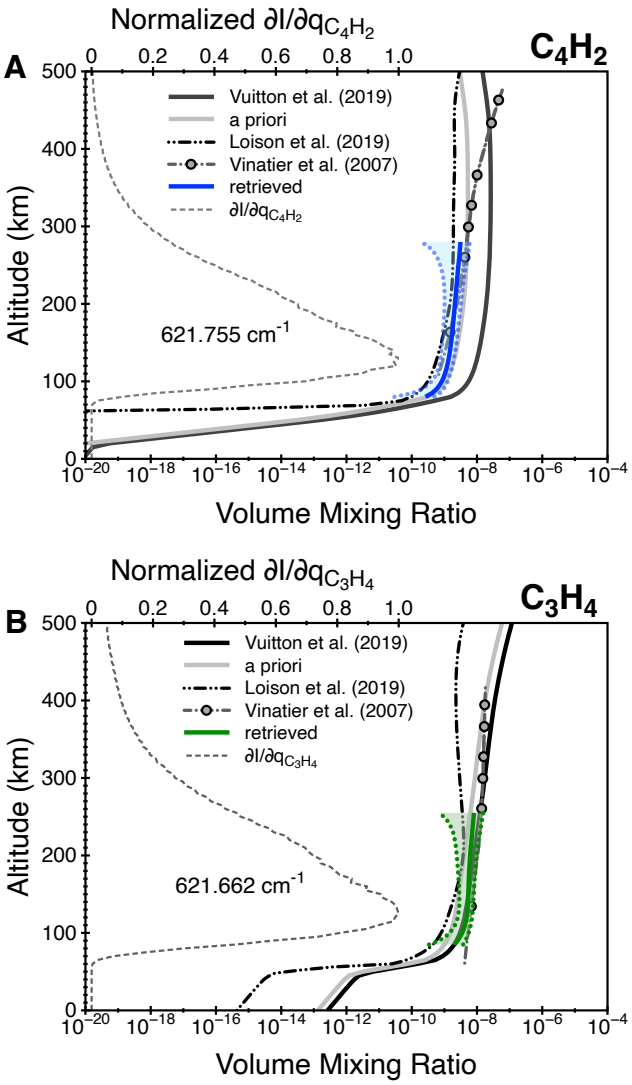

Figure 3. Retrieved stratospheric profiles (colored trace) of C_4H_2 (A) and C_3H_4 (B) and the photochemical model predictions from V. Vuitton et al. (2019; solid black trace) and J. Loison et al. (2015; dot-dotted–dashed trace). The scaled profile from V. Vuitton et al. (2019), used as the a priori reference profile, is shown in the solid gray trace. The retrieved profile from S. Vinatier et al. (2007) is also shown for comparison (gray points and dotted–dashed trace). Each panel also shows the Jacobian at $\bar{\nu}_{max}$ for each molecule to indicate the altitude range the model is sensitive to.

and increases sharply as the VMR increases above 10^{-11}. The upper limit values for both C_6H_2 and C_4N_2 are reported in Table 3. We find a 3σ upper limit on the uniform abundance of 4.29×10^{-11} for C_6H_2. Figure 4(B) shows the corresponding spectra from each abundance at 1σ, 2σ, and 3σ upper limits. There is a clear growth in the radiance due to the ν_{11} vibrational mode of C_6H_2, indicated by the black triangle markers. The three main emission features in these spectra lie near strong emission features from C_4H_2, highlighting the importance of using the high-resolution capabilities of EXES. These emission features from C_6H_2 would have been smoothed together with emission features from C_4H_2 with lower-resolution spectrometers such as CIRS or IRIS, requiring a much higher abundance of C_6H_2 to deviate significantly from the measurement and consequentially leading to higher upper limits.

A uniform vertical profile above 125 km was used to determine the upper limits to the abundance of gas phase C_4N_2 based on the saturation vapor pressures reported in N. Fray & B. Schmitt (2009), which were extrapolated to Titan's stratospheric temperatures. This cutoff altitude is similar to the upper limit study by A. Jolly et al. (2015), who applied a similar method for determining the cutoff altitude for the uniform profile. Figure 4 (C) shows the $\Delta\chi^2$ increases sharply with VMR. We determine a 3σ upper limit on the abundance of 9.96×10^{-11}. Figure 4(D) shows the many emission features originating from the ν_8 bending mode of C_4N_2, which is very dense with many emission lines. This high density of emission features provides strong statistical evidence for the rejection of C_4N_2 presence in the measurement, as each peak in the simulated spectra contributes to the total χ^2 of the model.

5. Discussion

5.1. C_6H_2

Previous attempts at detecting C_6H_2 in Titan's atmosphere have ultimately led to nondetection and upper-limit determinations of the abundance. Figure 5 shows the upper limits determined from this study in comparison with those from C. Delpech et al. (1994) and F. Shindo et al. (2003). The new upper limits improve upon the previous ones by over an order of magnitude. This can be attributed to the high resolution of EXES, which can resolve individual emission features in a small wavenumber range that may have previously been blended together at lower resolutions. Figure 5 also compares the present results with photochemical model predictions of the vertical C_6H_2 profile. Comparing to the V. Vuitton et al. (2019) profile of the C_6H_2 abundance, these upper limits are significantly lower than the predicted stratospheric abundance. We derived a scale factor of the V. Vuitton et al. (2019) profile of 0.093.

Included in Figure 5 is a vertical profile from an updated photochemical model for both C_6H_2 and C_4N_2 shared in a private communication by Panayotis Lavvas (P. Lavvas 2025, private communication; red trace in Figure 5). These profiles are the results of a model similar to that presented in V. Vuitton et al. (2019), which is a 1D photochemical model of Titan's atmosphere including neutral and ionic chemical processes (P. Lavvas et al. 2008a, 2021). In addition to the model described in P. Lavvas et al. (2008a), the model includes high-resolution description of the energy deposition in Titan's upper atmosphere through solar photons (P. Lavvas et al. 2011), and the contribution of the photochemical haze opacity in the radiation transfer in Titan's atmosphere based on measurements made by the Huygens Descent Imager/Spectral Radiometer (P. Lavvas et al. 2010). The photochemical model also accounts for the escape of atomic and molecular hydrogen according to the Jean escape rate, and methane is allowed to escape at a fixed velocity of 100 cm s^{-1} to match the observed profiles of methane and argon in the upper atmosphere based on measurements made by the Ion Neutral Mass Spectrometer during the Cassini–Huygens mission (P. Lavvas et al. 2008b; R. V. Yelle et al. 2008).

The low upper limit for C_6H_2 in this work, combined with a lower retrieved abundance of its precursor, C_4H_2, suggests that loss mechanisms for C_4H_2 are not being fully represented in V. Vuitton et al. (2019). C_4H_2 can be lost in Titan's atmosphere through combination with atomic hydrogen (H + C_4H_2; V. Vuitton et al. 2012, 2019). The Lavvas (2025) model

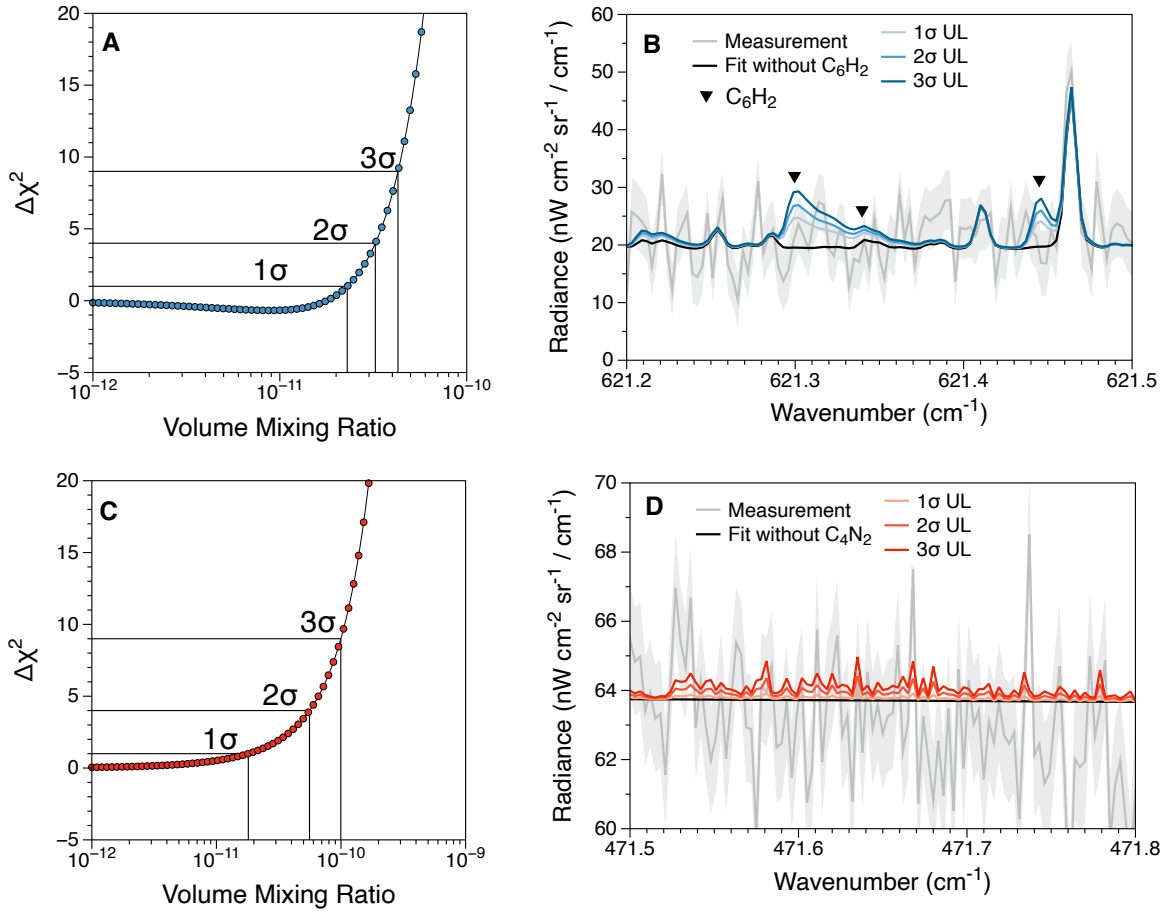

Figure 4. (A) The $\Delta\chi^2$ plotted as a function of the VMR for the uniform profile of C_6H_2 and (B) the corresponding simulated spectra for the 1σ, 2σ, and 3σ upper limits with C_6H_2 peaks indicated by the black triangle markers. (C)–(D) The $\Delta\chi^2$ and corresponding spectra for the upper limits of C_4N_2. All emission features in panel (D) are due to C_4N_2.

Table 3
Upper Limits for C_6H_2 and C_4N_2

Species	NESR 1σ (nW cm^{-2} sr^{-1} cm)	Volume Mixing Ratio 1σ	Volume Mixing Ratio 2σ	Volume Mixing Ratio 3σ	Column Density 3σ (m^{-2})
C_6H_2	1.028	$<2.30 \times 10^{-11}$	$<3.24 \times 10^{-11}$	$<4.29 \times 10^{-11}$	$<1.69 \times 10^{14}$
C_4N_2	1.003	$<1.80 \times 10^{-11}$	$<5.58 \times 10^{-11}$	$<9.96 \times 10^{-11}$	$<1.94 \times 10^{14}$

prediction presented here does not include a heterogeneous loss mechanism of H to haze particle surfaces, described in Y. Sekine et al. (2008), enriching the H abundance and decreasing the C_4H_2 abundance compared to V. Vuitton et al. (2019). Consequentially, this leads to a lower predicted C_6H_2 abundance as shown in Figure 5, which is in closer agreement with the present upper limits. Furthermore, additional loss of C_4H_2 could occur through the reaction with 1,3-butadiene (C_4H_6 isomer). I. A. Medvedkov et al. (2025) recently showed through crossed molecular beam experiments that the C_4H radical can add directly to 1,3-butadiene or 2-methyl-1,3-butadiene followed by isomerization to form aromatic rings. Additionally, C_2H_2 has been shown to react with HCO+ to initiate a cascade of chemical reactions ultimately leading to the formation of benzene (E. O. Pentsak et al. 2024). HCO+ has not been detected in Titan's atmosphere but is present in models of Titan's oxygen cycle (S. M. Hörst et al. 2008; M. Dobrijevic et al. 2016). Such reactions that form aromatics from C_2H_2 and C_4H_2 have not been well studied under Titan relevant conditions, but represent other potential loss mechanisms for the precursors to polyyne propagation in Titan's atmosphere. This suggests that polyyne propagation is not a suitable pathway to larger hydrocarbons or organic aerosols in Titan's atmosphere.

5.2. C_4N_2

The assignment of the emission feature at 478 cm^{-1} to ice-phase C_4N_2 in both Voyager's IRIS data (R. Samuelson et al. 1997) and CIRS data (C. M. Anderson et al. 2016) has led to many studies attempting to understand the lack of gas phase C_4N_2 in the spectra of Titan's atmosphere. Several upper limits have been determined, including the most stringent ones from A. Jolly et al. (2015), who found a 3σ upper limit on the stratospheric abundance of 1.5×10^{-9} using both CIRS nadir and limb observations of Titan's atmosphere. Figure 5(B) shows the 3σ upper limit presented in this study (gray square)

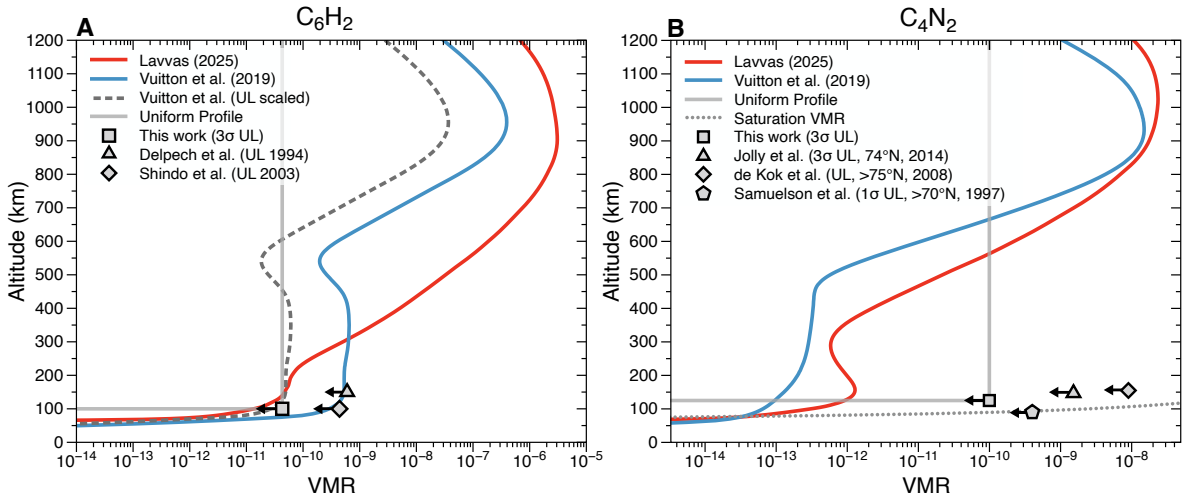

Figure 5. The 3σ upper limits found for this study (gray squares) for C_6H_2 (A) and C_4N_2 (B), along with previous studies of the upper limits. Also included are the photochemical model vertical profiles of each species (red and blue traces), the uniform profiles used for the upper limits (gray solid trace), and the scaling factor for the V. Vuitton et al. (2019) C_6H_2 profile (gray dashed trace). The gray dotted line in panel (B) is the saturation altitude calculated using the V. Vuitton et al. (2019) temperature profile and equation for the saturation vapor pressures in N. Fray & B. Schmitt (2009).

in comparison with previous estimations of the C_4N_2 gas phase upper limits (gray points). The upper limits of this study lower the upper limits of the gas phase C_4N_2 abundance by an order of magnitude. This improvement largely stems from the high resolution of EXES, where the individual emission features of the C_4N_2 ν_8 vibrational mode can be resolved. In previous studies of the upper limits, the lower resolution of CIRS and IRIS smooth the entire band into one peak, dampening the contribution of each line to the $\Delta\chi^2$. Figure 5(B) also compares the upper limits here to the photochemical model of V. Vuitton et al. (2019) and the aforementioned Lavvas (2025) model. The photochemical models predict an abundance of C_4N_2 gas in the stratosphere between $\sim 10^{-13}$ and 10^{-12}, which is substantially lower than the upper limits presented here.

Also present in Figure 5(B) are the altitudes at which C_4N_2 gas should condense (gray dotted line) based on the saturation vapor pressure temperatures presented in N. Fray & B. Schmitt (2009). We calculated the saturation mixing ratios based on the temperature profile used in this study (V. Vuitton et al. 2019) using the empirical definition of the saturation vapor pressure of C_4N_2 gas in N. Fray & B. Schmitt (2009). The temperature changes dramatically with altitude in the stratosphere which leads to a rapid increase in the saturation mixing ratio with altitude, hence the flat nature of the trace. We find that the upper limits presented here, calculated at 125 km, are below the saturation mixing ratio of C_4N_2 at this altitude, which suggests that ice nucleation is not likely.

This updated value for the upper limit, however, was determined from a disk averaged measurement, which is more sensitive to changes in the abundance at the equator, where trace gas concentrations in Titan's atmosphere tend to be diminished (N. A. Teanby et al. 2008; S. Vinatier et al. 2020). If C_4N_2 is present in lower abundances, it is possible still that it could be enriched in the polar regions of Titan during winter seasons. Titan's winter poles, however, are not visible from Earth, restricting the opportunities for improving searches for C_4N_2 gas by observing in regions where it may be enriched. The current proposed mechanism of C_4N_2 formation is that C_4N_2 ice is formed totally in the solid state through UV induced photochemistry (C. M. Anderson et al. 2016). Based on this mechanism, C. M. Anderson et al. (2016) require a C_4N_2 column abundance of 10^{17} molecules cm^{-2} for C_4N_2, which is substantially larger than the present value of $\sim 2 \times 10^{14}$. This would suggest that the C_4N_2 ice is highly out of equilibrium with the gas phase and would need to be retained completely in the closed shell. Laboratory experiments studying more closely the gas and ice-phase partitioning of C_4N_2 ice formed in closed shells would be needed to better understand the feasibility of this disequilibrium.

6. Conclusions

This study presents spectra collected in the mid-infrared of Titan's atmosphere using EXES during the SOFIA mission. These spectra represent the lone study of Titan's atmosphere during the SOFIA mission but display the value of using high-resolution infrared spectroscopy for atmospheric studies. The spectra presented in this study showed spectral signatures for C_4H_2 and C_3H_4, which allowed for their continuous stratospheric profiles to be retrieved. We showed the C_3H_4 profile to be similar to that of V. Vuitton et al. (2019), but the C_4H_2 profile was lower than the photochemical model prediction. The target species, C_6H_2 and C_4N_2, were not detected; instead, we performed an upper limits study to the atmospheric abundances of the target species. The C_6H_2 upper limit, which has not been assessed since the Voyager mission (C. Delpech et al. 1994), was found to be lower than previous studies of C. Delpech et al. (1994) and F. Shindo et al. (2003) and constrains the photochemical model in V. Vuitton et al. (2019). We show that C_4H_2 is overpredicted in the V. Vuitton et al. (2019) model and ultimately leads to the overprediction of the C_6H_2 stratospheric abundance. This strict upper limit shows the potential for C_6H_2 formation and large polyyne propagation is low and the precursors are likely lost to other chemical processes.

Additionally, we lower the upper limit for C_4N_2 gas in Titan's atmosphere by an order of magnitude. This new value for the C_4N_2 upper limit shows that ice nucleation is unlikely to occur in Titan's atmosphere directly. The formation of C_4N_2 ice through solid-state photochemistry is still possible, though the ice would be substantially out of equilibrium with the gas

phase. Further work would be needed to better understand the gas-solid phase partitioning of C_4N_2 ice formed in an enclosed shell.

Acknowledgments

The material is based upon work supported by NASA under award No. 80GSFC24M0006. C.A.N. received support for his part of the work from NASA's CDAP and Astrobiology programs. N.A.T. is supported by UK Science and Technology Facilities Council grant ST/Y000676/1. This research was also supported by the International Space Science Institute (ISSI) in Bern through ISSI International Team project #24-615 (ATTACK).

ORCID iDs

Zachary C. McQueen https://orcid.org/0009-0006-1322-7652
Conor A. Nixon https://orcid.org/0000-0001-9540-9121
Panayotis Lavvas https://orcid.org/0000-0002-5360-3660
Juan Alday https://orcid.org/0000-0003-1459-3444
Nicholas A. Teanby https://orcid.org/0000-0003-3108-5775
Patrick G. J. Irwin https://orcid.org/0000-0002-6772-384X

References

Alday, J., Penn, J., Irwin, P., et al. 2025, archNEMESIS: An Open-source Python Package for Analysis of Planetary Atmospheric Spectra, JORS, 13, 10
Anderson, C. M., Samuelson, R. E., Yung, Y. L., & McLain, J. L. 2016, Solid-state Photochemistry as a Formation Mechanism for Titan's Stratospheric C4N2 Ice Clouds, GeoRL, 43, 3088
Broadfoot, A. L., Sandel, B. R., Shemansky, D. E., et al. 1981, Extreme Ultraviolet Observations from Voyager 1 Encounter with Saturn, Sci, 212, 206
Cernicharo, J., Heras, A. M., Pardo, J. R., et al. 2001a, Methylpolyynes and Small Hydrocarbons in CRL 618, ApJL, 546, L127
Cernicharo, J., Heras, A. M., Tielens, A. G. G. M., et al. 2001b, Infrared Space Observatory's Discovery of C4H2, C6H2, and Benzene in CRL 618, ApJL, 546, L123
Chassefière, E., & Cabane, M. 1995, Two Formation Regions for Titan's Hazes: Indirect Clues and Possible Synthesis Mechanisms, P&SS, 43, 91
Clarke, M., Vacca, W. D., & Shuping, R. Y. 2015, Redux: A Common Interface for SOFIA Data Reduction Pipelines, ASPC, 495, 355
Cordiner, M. A., Garcia-Berrios, E., Cosentino, R. G., et al. 2020, Detection of Dynamical Instability in Titan's Thermospheric Jet, ApJL, 904, L12
Cordiner, M. A., Teanby, N. A., Nixon, C. A., et al. 2019, ALMA Spectral Imaging of Titan Contemporaneous with Cassini's Grand Finale, AJ, 158, 76
Coustenis, A., Jennings, D., Nixon, C., et al. 2010, Titan Trace Gaseous Composition from CIRS at the End of the Cassini–Huygens Prime Mission, Icar, 207, 461
Coustenis, A., Salama, A., Lellouch, E., et al. 1998, Evidence for Water Vapor in Titan's Atmosphere from ISO/SWS Data, A&A, 336, L85
Coustenis, A., Salama, A., Schulz, B., et al. 2003, Titan's Atmosphere from ISO Mid-infrared Spectroscopy, Icar, 161, 383
de Aragão, E. V. F., Liang, P., Mancini, L., et al. 2025, Dicyanoacetylene (NC4N) Formation in the CN + Cyanoacetylene (HC3N) Reaction: A Combined Crossed-molecular Beams and Theoretical Study, ESC, 9, 2199
de Kok, R., Irwin, P., & Teanby, N. 2008, Condensation in Titan's Stratosphere during Polar Winter, Icar, 197, 572
Delahaye, T., Armante, R., Scott, N., et al. 2021, The 2020 Edition of the GEISA Spectroscopic Database, JMoSp, 380, 111510
Delpech, C., Guillemin, J., Paillous, P., et al. 1994, Infrared Spectra of Triacetylene in the 4000–220 cm1 Region: Absolute Band Intensity and Implications for the Atmosphere of Titan, AcSpA, 50, 1095
Dobrijevic, M., Loison, J., Hickson, K., & Gronoff, G. 2016, 1D-coupled Photochemical Model of Neutrals, Cations and Anions in the Atmosphere of Titan, Icar, 268, 313
Encrenaz, T. 2003, ISO Observations of the Giant Planets and Titan: What Have We Learnt?, P&SS, 51, 89
Fray, N., & Schmitt, B. 2009, Sublimation of Ices of Astrophysical Interest: A Bibliographic Review, P&SS, 57, 2053
Gordon, I., Rothman, L., Hargreaves, R., et al. 2022, The HITRAN2020 Molecular Spectroscopic Database, JQSRT, 277, 107949
Gu, X., Kim, Y. S., Kaiser, R. I., et al. 2009, Chemical Dynamics of Triacetylene Formation and Implications to the Synthesis of Polyynes in Titan's Atmosphere, PNAS, 106, 16078
Hanel, R., Conrath, B., Flasar, F. M., et al. 1981, Infrared Observations of the Saturnian System from Voyager 1, Sci, 212, 192
Hörst, S. M. 2017, Titan's Atmosphere and Climate, JGRE, 122, 432
Hörst, S. M., Vuitton, V., & Yelle, R. V. 2008, Origin of Oxygen Species in Titan's Atmosphere, JGRE, 113, E10006
Irwin, P., Teanby, N., Kok, R., et al. 2008, The NEMESIS Planetary Atmosphere Radiative Transfer and Retrieval Tool, JQSRT, 109, 1136
Jolly, A., Cottini, V., Fayt, A., et al. 2015, Gas Phase Dicyanoacetylene (C4N2) on Titan: New Experimental and Theoretical Spectroscopy Results Applied to Cassini Cirs Data, Icar, 248, 340
Jolly, A., Manceron, L., Kwabia-Tchana, F., Benilan, Y., & Gazeau, M.-C. 2014, Revised Infrared Bending Mode Intensities for Diacetylene (C4H2): Application to Titan, P&SS, 97, 60
Kuiper, G. P. 1944, Titan: A Satellite with an Atmosphere, ApJ, 100, 378
Kunde, V. G., Aikin, A. C., Hanel, R. A., et al. 1981, C4H2, HC3N and C2N2 in Titan's Atmosphere, Natur, 292, 686
Lavvas, P., Coustenis, A., & Vardavas, I. 2008a, Coupling Photochemistry with Haze Formation in Titan's Atmosphere, Part I: Model Description, P&SS, 56, 27
Lavvas, P., Coustenis, A., & Vardavas, I. 2008b, Coupling Photochemistry with Haze Formation in Titan's Atmosphere, Part II: Results and Validation with Cassini/Huygens Data, P&SS, 56, 67
Lavvas, P., Galand, M., Yelle, R., et al. 2011, Energy Deposition and Primary Chemical Products in Titan's Upper Atmosphere, Icar, 213, 233
Lavvas, P., Lellouch, E., Strobel, D. F., et al. 2021, A Major Ice Component in Pluto's Haze, NatAs, 5, 289
Lavvas, P., Yelle, R., & Griffith, C. 2010, Titan's Vertical Aerosol Structure at the Huygens Landing Site: Constraints on Particle Size, Density, Charge, and Refractive Index, Icar, 210, 832
Lebonnois, S., Bakes, E., & McKay, C. P. 2002, Transition from Gaseous Compounds to Aerosols in Titan's Atmosphere, Icar, 159, 505
Letourneur, B., & Coustenis, A. 1993, Titan's Atmospheric Structure from Voyager 2 Infrared Spectra, P&SS, 41, 593
Loison, J., Dobrijevic, M., & Hickson, K. 2019, The Photochemical Production of Aromatics in the Atmosphere of Titan, Icar, 329, 55
Loison, J., Hébrard, E., Dobrijevic, M., et al. 2015, The Neutral Photochemistry of Nitriles, Amines and Imines in the Atmosphere of Titan, Icar, 247, 218
Lombardo, N. A., Nixon, C. A., Achterberg, R. K., et al. 2019a, Spatial and Seasonal Variations in C3Hx Hydrocarbon Abundance in Titan's Stratosphere from Cassini CIRS Observations, Icar, 317, 454
Lombardo, N. A., Nixon, C. A., Greathouse, T. K., et al. 2019b, Detection of Propadiene on Titan, ApJL, 881, L33
Maguire, W. C., Hanel, R. A., Jennings, D. E., Kunde, V. G., & Samuelson, R. E. 1981, C3H8 and C3H4 in Titan's Atmosphere, Natur, 292, 683
Medvedkov, I. A., Yang, Z., Nikolayev, A. A., et al. 2025, Binding the Power of Cycloaddition and Cross-coupling in a Single Mechanism: An Unexpected Bending Journey to Radical Chemistry of Butadiynyl with Conjugated Dienes, JPCL, 16, 658
Nixon, C. A. 2024, The Composition and Chemistry of Titan's Atmosphere, ESC, 8, 406
Nixon, C. A., Achterberg, R. K., Teanby, N. A., et al. 2010, Upper Limits for Undetected Trace Species in the Stratosphere of Titan, FaDi, 147, 65
Nixon, C. A., Ansty, T. M., Lombardo, N. A., et al. 2019, Cassini Composite Infrared Spectrometer (CIRS) Observations of Titan 2004–2017, ApJS, 244, 14
Nixon, C. A., Bézard, B., Cornet, T., et al. 2025, The Atmosphere of Titan in Late Northern Summer from JWST and Keck Observations, NatAs, 9, 969
Nixon, C. A., Jennings, D. E., Bézard, B., et al. 2013, Detection of Propene in Titan's Stratosphere, ApJL, 776, L14
Nixon, C. A., Thelen, A. E., Cordiner, M. A., et al. 2020, Detection of Cyclopropenylidene on Titan with ALMA, AJ, 160, 205
Palmer, M. Y., Cordiner, M. A., Nixon, C. A., et al. 2017, ALMA Detection and Astrobiological Potential of Vinyl Cyanide on Titan, SciA, 3, e1700022
Pekkala, K. 1990, The 9 Band of Propyne, JMoSp, 144, 416

Pentsak, E. O., Murga, M. S., & Ananikov, V. P. 2024, Role of Acetylene in the Chemical Evolution of Carbon Complexity, ESC, 8, 798
Richter, M. J., DeWitt, C. N., McKelvey, M., et al. 2018, EXES: The Echelon-cross-echelle Spectrograph for SOFIA, JAI, 07, 1840013
Samuelson, R., Mayo, L., Knuckles, M., & Khanna, R. 1997, C4N2 Ice in Titan's North Polar Stratosphere, P&SS, 45, 941
Samuelson, R. E., Maguire, W. C., Hanel, R. A., et al. 1983, CO2 on Titan, JGRA, 88, 8709
Sekine, Y., Lebonnois, S., Imanaka, H., et al. 2008, The Role of Organic Haze in Titan's Atmospheric Chemistry. II. Effect of Heterogeneous Reaction to the Hydrogen Budget and Chemical Composition of the Atmosphere, Icar, 194, 201
Shindo, F., Benilan, Y., Guillemin, J.-C., et al. 2003, Ultraviolet and Infrared Spectrum of C6H2 Revisited and Vapor Pressure Curve in Titan's Atmosphere, P&SS, 51, 9
Teanby, N., Irwin, P., Kok, R., et al. 2008, Global and Temporal Variations in Hydrocarbons and Nitriles in Titan's Stratosphere for Northern Winter Observed by Cassini/CIRS, Icar, 193, 595
Teanby, N., Irwin, P., Kok, R., et al. 2009, Titan's Stratospheric C2N2, C3H4, and C4H2 Abundances from Cassini/CIRS Far-infrared Spectra, Icar, 202, 620
Teanby, N., Irwin, P., Nixon, C., et al. 2013, Constraints on Titan's Middle Atmosphere Ammonia Abundance from Herschel/SPIRE Sub-millimetre Spectra, P&SS, 75, 136
Teanby, N. A., Kok, R., Irwin, P. G. J., et al. 2008, Titan's Winter Polar Vortex Structure Revealed by Chemical Tracers, JGRE, 113, E12003
Teanby, N. A., Sylvestre, M., Sharkey, J., et al. 2019, Seasonal Evolution of Titan's Stratosphere during the Cassini Mission, GeoRL, 46, 3079
Terragni, J., Gordon, I., Adkins, E., et al. 2025, Collision Induced Absorption in HITRAN2024: Enhanced and Improved Data for Atmospheric and Planetary Studies, JQSRT, 347, 109631
Thelen, A. E., Nixon, C. A., Cordiner, M. A., et al. 2019, Measurement of CH3D on Titan at Submillimeter Wavelengths, AJ, 157, 219
Trainer, M. G., Pavlov, A. A., DeWitt, H. L., et al. 2006, Organic Haze on Titan and the Early Earth, PNAS, 103, 18035
Villanueva, G. L., Smith, M. D., Protopapa, S., Faggi, S., & Mandell, A. M. 2018, Planetary Spectrum Generator: An Accurate Online Radiative Transfer Suite for Atmospheres, Comets, Small Bodies and Exoplanets, JQSRT, 217, 86
Vinatier, S., Bézard, B., Fouchet, T., et al. 2007, Vertical Abundance Profiles of Hydrocarbons in Titan's Atmosphere at 15°S and 80°N Retrieved from Cassini/CIRS Spectra, Icar, 188, 120
Vinatier, S., Bézard, B., Lebonnois, S., et al. 2015, Seasonal Variations in Titan's Middle Atmosphere during the Northern Spring Derived from Cassini/CIRS Observations, Icar, 250, 95
Vinatier, S., Mathé, C., Bézard, B., et al. 2020, Temperature and Chemical Species Distributions in the Middle Atmosphere Observed during Titan's Late Northern Spring to Early Summer, A&A, 641, A116
Vuitton, V., Yelle, R., Klippenstein, S., Hörst, S., & Lavvas, P. 2019, Simulating the Density of Organic Species in the Atmosphere of Titan with a Coupled Ion-neutral Photochemical Model, Icar, 324, 120
Vuitton, V., Yelle, R. V., Lavvas, P., & Klippenstein, S. J. 2012, Rapid Association Reactions at Low Pressure: Impact on the Formation of Hydrocarbons on Titan, ApJ, 744, 11
Waite, J. H., Jr., Young, D. T., Cravens, T. E., et al. 2007, The Process of Tholin Formation in Titan's Upper Atmosphere, Sci, 316, 870
Wright, L., Teanby, N. A., Irwin, P. G. J., & Nixon, C. A. 2024, Forward Modelling Low-spectral-resolution Cassini/CIRS Observations of Titan, ExA, 57, 15
Wright, L., Teanby, N. A., Irwin, P. G. J., et al. 2025, Seasonal Evolution of Titan's Stratospheric Tilt and Temperature Field at High Resolution from Cassini/CIRS, PSJ, 6, 114
Yelle, R. V., Cui, J., & Müller-Wodarg, I. C. F. 2008, Methane Escape from Titan's Atmosphere, JGRE, 113, E10003